MORGen: an Algorithm to Compute Spreading Centre and Transform Geometries from Simple Initial Plate Boundaries and Euler Rotations

Thomas J. M. van der Linden [iD] [*1], **Douwe J. J. van Hinsbergen** [iD][1]

[1]Department of Earth Sciences, Utrecht University, Princetonlaan 8A, 3584 CB Utrecht, the Netherlands

Abstract   The age structure of the global ocean floor is a key feature in paleogeographic reconstructions, which in turn forms the quantitative basis for Earth System Science. However, much of the ocean floor in paleogeographic reconstructions has been lost to subduction. The age structure of such lost ocean floor is constructed from the reconstructions of adjacent continents, using the relative rotations, around Euler poles to predict the geometry of spreading centres and transform faults. Building such mid-ocean ridge features in paleogeographic reconstructions is laborious, as it requires redrawing of ridge-transform systems upon every Euler pole shift in the model. In this paper, we present the Mid-Ocean Ridge Generator (MORGen) algorithm, based on pyGPlates. MORGen reduces the laborious task by automating the drawing of mid-ocean ridge geometries from geometrically simple plate boundary input assuming ridge-perpendicular spreading and adjusts ridge geometries in a simplest-scenario fashion by gradually adjusting ridge orientation and transform fault length upon Euler pole shifts, inspired by observations from the modern sea floor. The code takes as input curved line features, representing approximate divergent plate boundaries, and a set of Euler poles. These are then converted into spreading centre-transform geometries. Upon Euler pole shifts, the geometries are adjusted to fit the set of small circles and great circles dictated by the new Euler pole. For studies of paleo-environment and paleo-oceanography MORGen can be used in combination with other algorithms for full reconstructions of ocean floors, including their age, bathymetry, and roughness. For in-situ preserved ocean floor, the paleo-age distribution can be reconstructed directly in high resolution from geophysical and geological data from the modern ocean floor and MORGen would not normally be the option of choice. In cases where models contain ocean floor that has now been subducted, MORGen straightforwardly facilitates mid-ocean ridge geometry reconstruction. To illustrate how well the MORGen algorithm reproduces real ocean floor age structure, we show a synthetic ridge evolution for the South Atlantic and Southern Oceans and compare this to geophysically constrained ocean floor geometry. In addition, we show examples of use cases where direct (re)construction of mid ocean ridges is not possible: now-subducted ocean basins in the Mediterranean region and an ocean in a future supercontinent scenario.

1 Introduction

Paleogeographic reconstructions display the distribution in the geological past of continents and oceans, which provide key input for Earth System Science (e.g., *Torsvik and M. Cocks*, 2016). Classically, such models contain information on full-plate evolution back to times of Pangea, but for older times, no ocean floor is left that allows the data-based reconstruction of mid-ocean ridges and transforms. Essentially, pre-Pangean paleogeographical reconstructions are 'continental drift' models, in which only the relative positions of continents and arcs that are preserved in the geological record are displayed, separated by oceans from which little information remains (e.g., *Torsvik and M. Cocks*, 2016). However, if the relative motions of adjacent continents are reconstructed, the age structure of the oceans between those continents can be forward modelled (*Karlsen et al.*, 2020; *Merdith et al.*, 2019; *Seton et al.*, 2012; *Williams et al.*, 2021).

In the last decade, the free plate reconstruction software GPlates (*Boyden et al.*, 2011; *Müller et al.*, 2018) has become widely used to develop full-plate reconstructions, as far back as 1.5 Ga, and these include such conceptually modelled mid-ocean ridges in oceans that have been lost to subduction (e.g., *Domeier and Torsvik*, 2014, 2019; *Domeier*, 2016, 2018; *Matthews et al.*, 2016; *Müller et al.*, 2016; *Young et al.*, 2018; *Merdith et al.*, 2017, 2021). Constructing mid-ocean ridges with spreading centre and transform fault segments (Figure 1) at high resolution is currently time-consuming: not only is each ridge drawn by hand along great circles and small circles, but because the orientation of such great circles and small circles changes with each change of Euler poles, the model ridges also have to be redrawn at each Euler pole shift. This redrawing leads to abrupt ridge
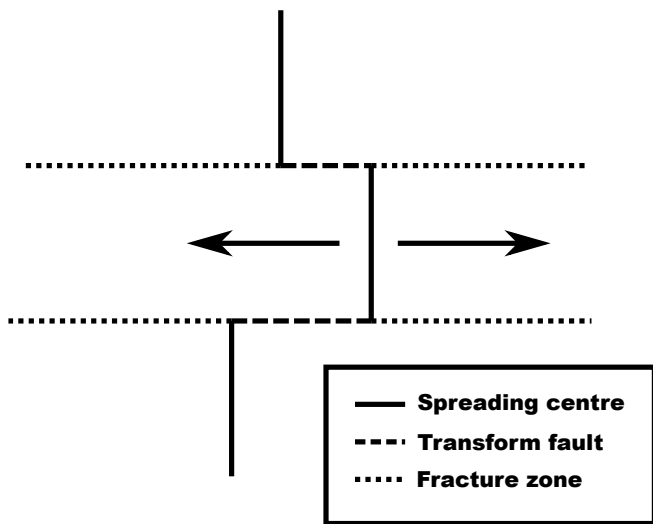
*✉ thomas@lingeo.eu

Figure 1 – Terminology of mid-ocean ridges used in this paper

jumps in the model. However, documented expressions on the modern ocean floor show that Euler pole shifts are common and are typically accommodated by gradual changes in transform fault and spreading centre strike, and associated changes in spreading centre and transform spacing (*Menard and Atwater*, 1968), as evidenced by s-shaped transform fault traces, visible for instance between Africa and Antarctica in Figure 2, rather than by ridge jumps. And even though ridge jumps occasionally occur, inferring ridge jumps for each Euler pole shift unnecessarily complicates plate models. These ridge jumps introduce new plate boundaries, which is especially inconvenient if the model contains topologically closed plate boundaries, in which gradually evolving plate shapes are determined from intersecting, moving plate boundaries (*Gurnis et al.*, 2018), because each Euler pole shift then requires the recreation of topologies. This is laborious and hampers visual analysis of full-plate models.

Reconstructing mid-ocean ridges between diverging plates is conceptually straightforward using principles of plate tectonics (*Atwater and Macdonald*, 1977; *Cox and Hart*, 1986; *McKenzie and Parker*, 1967; *Morgan*, 1991; *Wilson*, 1965): (i) spreading centres form parallel to great circles through Euler poles that describe the relative motion between two diverging plates; (ii) spreading centres are connected through transform faults (which connect two inactive, within-plate fracture zones) that form along small circles around these poles, and (iii) assuming symmetric spreading, spreading centres migrate at half-spreading rate away from the adjacent plates. Originally curvilinear rifts displayed in plate models, e.g. based on conjugate margin shapes (e.g., ocean-continent transitions), thus develop into the stepped geometry with spreading centres connected through transforms that are so characteristic of modern mid-ocean ridges (Figure 1), while the continental margins maintain the original curvilinear shape (Figure 2) (see e.g., *Gerya*, 2010).

In this paper, we introduce an algorithm that computes evolving mid-ocean ridge systems, out of an initial estimated rift orientation, that gradually adjusts orientation during Euler pole shifts conform to known characteristics of mid-ocean ridges. We also introduce additional tools that can support creating full ocean floor reconstructions from these mid-ocean ridge geometries. We first briefly review typical geometries and dimensions of modern ridges, and how these change over time in Section 2. We substantiate that the algorithm is effective in Section 4.1 and illustrate the applicability, and the simplifications associated with the algorithm by synthetically recalculating pseudo-isochrons for some modern ocean basins from the set of Euler poles reconstructing their opening, using only initial ridge/rift geometry as input in Section 4.2. Finally, we illustrate the tool with examples of pseudo-isochrons and age grids for ocean basins in reconstructions of the Neotethyan realm, as well as oceans in constructions of a future plate tectonic scenario in Section 4.3.

2 Modern mid-ocean ridge geometries

Most existing mid-ocean ridges started their lives as rifts in continents that broke up (e.g., *Seton et al.* (2012), but see *Boschman and van Hinsbergen* (2016) for an exception). The philosophy behind the algorithm is to follow the development of mid-ocean ridges from their inception, using the rift (after it has developed into continental plate boundaries) as a basis for initial ridge geometry, and create spreading centre and transform segments on that geometry according to subsequent Euler pole shifts and rotation rate. The typical stepped geometry of mid-ocean ridges in 2D top view develops with progressing spreading from the generally smooth curves of rift geometries (*Bosworth*, 1985). Relay ramps between normal fault segments, or pre-existing fault structures, develop into transform faults that are parallel to the spreading direction and that connect spreading centres (*Gerya*, 2010). Spreading centres accommodate divergence and are generally perpendicular to the spreading direction (*Atwater and Macdonald*, 1977; *Seton et al.*, 2020). A typical shape of a mid-ocean ridge is illustrated in Figure 2 for the South Atlantic Ocean.

Changes in spreading direction, which are expressed as shifts of the Euler pole that describes the plate divergence, lead to smooth curves of continuous transform fault-fracture zones from the old to the new orientation. Occasionally, such changes can instead be associated with ridge jumps as has been well-documented from the modern ocean floor (e.g., *Labrecque and Hayes*, 1979; *Luhr et al.*, 1985; *Marks and Stock*, 2001): during such times, a ridge segment is abandoned and a new ridge segment initiates within one of the two plates. This then leads to a transfer of a fragment of lithosphere from one plate to the other. But while such complex behaviour may
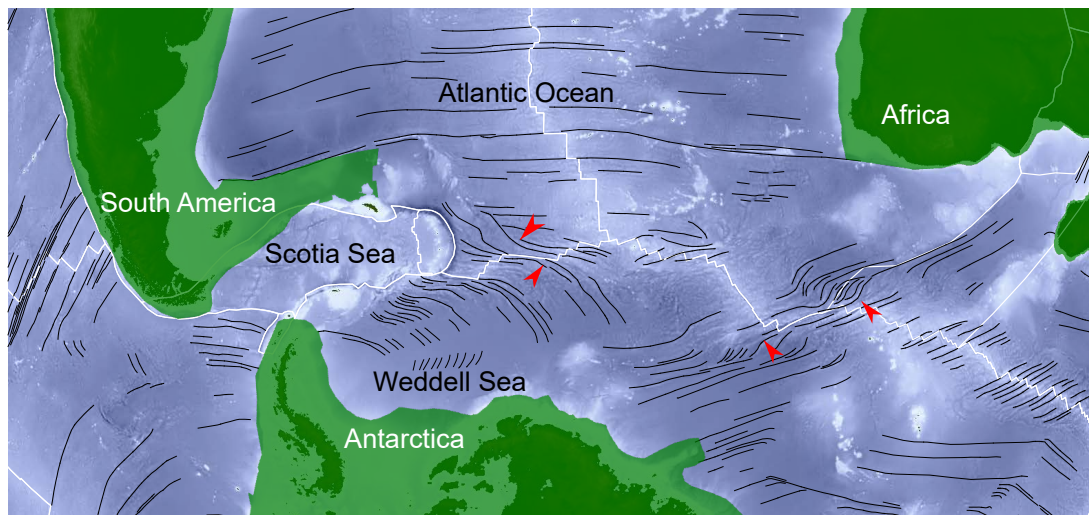
Figure 2 – Orientation change in transforms. Black: fracture zones (*Seton et al.*, 2012, and references therein); white: plate boundaries *Bird* (2003), red arrows point out s-shaped transform fault traces. Background bathymetry from ETOPO, oceans coloured blue, continents coloured green, using *Seton et al.* (2012) polygons.

also occur at small scale (e.g., in the South China Sea (*Guan et al.*, 2021), the gradual and smooth curves in fracture zones displayed in Figure 2 illustrate that changes in Euler pole location are typically associated with gradual orientation adjustments of mid-ocean ridge segments. Thus, the general shape of the plate boundary does not appear to jump when an Euler pole shift occurs, but orientations and lengths of the spreading centres and transforms are adjusted. This behaviour can be seen in e.g., the curved fault zones in the Weddell Sea and in the sigmoidal fault zones on the ocean floor between Africa and Antarctica (Figure 2). In reconstructions of lost ocean basins based on Euler poles estimated from continental records, the simplest scenario is thus to model plate boundaries as gradually changing rather than jumping and transferring lithosphere from one plate to the other upon each jump.

3 Method

The algorithm is written in Python (*Van Rossum and Drake*, 2011) and relies on GPlates and pyGPlates (*Müller et al.*, 2018) for its core, together with commonly used Python libraries (see Supporting Information, Section SI-1). Vector output data are produced in the GPlates markup language (gpml) format, as line and polygon features, non-raster data. The conversion from vector data to rasterized age grids and bathymetry grids are made with help of GMT (*Wessel et al.*, 2013). Grids are produced in the international standard NetCDF (*Unidata*, 2021) using standard time increments of 5 or 10 Myr and at a spatial resolution of 0.5 degree. Both are variables that can be set by the user.

3.1 Core of the Algorithm: Creating mid-Oceanic Ridge Geometries with Spreading Centre and Transform Fault Segments

To compute stepped, discrete ridges out of rifts of distributed extension that we represent as smooth curves, the code takes the following steps. The algorithm takes as input a kinematic (GPlates compatible) plate model in which each mid-ocean ridge is defined as a curvilinear plate boundary (Figure 3A). Such a boundary may either represent a rift at the initiation of spreading such as reconstructed for e.g., the southern Atlantic Ocean (e.g., *Torsvik et al.*, 2009), but also may represent an estimated, approximate geometry of the plate boundary in deep-time full-plate reconstructions (e.g., *Domeier*, 2016; *Merdith et al.*, 2021). In GPlates, such curves are defined as a line connecting a set of user-defined points with a latitude and a longitude. The divergence history of the plates adjacent to the ridge should be given by a set of total reconstruction poles for the lifetime of the ridge. Our code then subdivides the curve to increase its resolution such that there is not more than ~70 km between points on the line (Figure 3B). We chose this distance based on the modern median spacing between transform faults. We calculated the typical lengths of segments of the mid-ocean ridges from the data set of *Bird* (2003) and found a median length of 74 km of present-day spreading centres between two transform fault segments (see Tables in Supporting Information). We applied this estimate for our analysis but spacing can be adjusted by the user. The set of total reconstruction poles is translated into stage poles for a user-defined, but default 10 Ma time interval from the onset of spreading, and a small circle segment around the first stage pole is then drawn at each point defining the line (black lines in Figure 3C). These small circles define the transform fault segments, and the intersection points of the curve with the transforms drawn at the first time interval will ex-
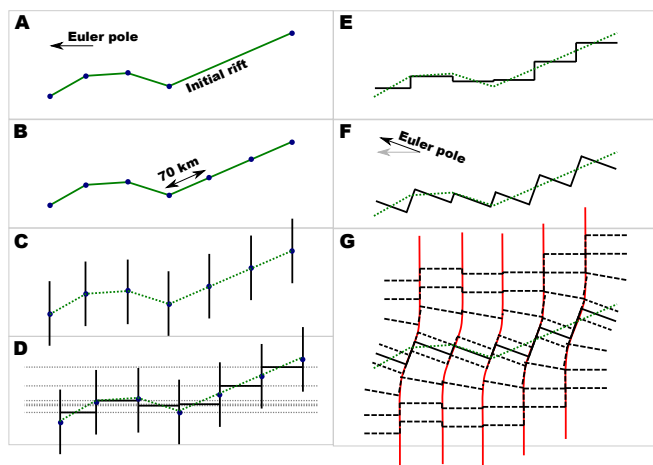
Figure 3 – Schematic depiction of the steps taken by the algorithm. **A)** shows an input feature from the model, representing an initial rift (as a green line, defined by the blue points). This can be considered as a snapshot of a moment in which the initial rift has not yet developed into a mid-ocean ridge. The Euler pole is located to the left and plate motions are oriented towards top and bottom of this figure; **B)** The feature is subdivided by adding extra points, so that the maximum distance between two adjacent points is 70 km, this is the approximate average distance between transform faults in the current oceans; **C)** line segments parallel to small circles of the Euler pole (drawn black lines oriented vertically in this figure) are added at each point on the line feature, these will later form the transform fault segments; **D)** great circles are added (horizontal lines in this figure), these are defined by the Euler pole and a point in between each of the drawn points. Only the segments (drawn in black) in between the corresponding transform faults are stored, not the segments (drawn as dotted lines) outside the corresponding transform faults. The transform segments are also clipped so as to only exist between ridges segments; **E)** the original (hand) drawn feature (green dotted line) is shown together with the calculated mid-ocean ridge geometry consisting of spreading centres and transform faults (black drawn line); **F)** upon a shift of the Euler pole from straight left to top left, steps 3A-3E are repeated to create the mid-ocean ridge geometry consisting of spreading centres and transform faults with a new orientation matching the new location of the Euler pole; **G)** from only the initial rift and changing Euler poles as input, the development of the mid-ocean ridge through time follows from the synthetic pseudo-isochrons (black striped lines, the active mid-ocean ridge is drawn in black). The red lines in this figure were added to illustrate the curving nature of the resulting fracture zones as a result of changes in Euler poles, these are not produced by the algorithm.

ist throughout the lifetime of the ridge. In the exceptional case that initial rifts are perfectly perpendicular to the initial divergence direction, transforms are also defined but will have a length equal to zero (Figure 3C). Then, the code draws spreading centres for each segment between two points on the initial curve: for each segment a great circle (dotted line in Figure 3D) is drawn through the first stage pole and its antipole, and with a longitude such that the shortest distance of the great circle to the two points on the line is equal (Figure 3D). The intersections of the small circles and great circles are then combined to

one line with the typical stepped geometry of a mid-ocean ridge (Figure 3E). Pseudo-isochrons are then drawn for each stage pole by repeating the above steps. If within such a time interval the location of the Euler pole shifted, the mid-ocean ridge is automatically redrawn with the new constraints. Because the points at which the transforms are drawn remain the same, an Euler pole shift means that the spacing between the transform faults, and the lengths of spreading centres will change, but that the originally defined transforms will remain (Figure 3F). Upon Euler pole shifts, transforms that had a length equal to zero will generate an offset and become visible as a 'new' transform fault, similar to natural examples (e.g. Figure 2). The final construction then has a permanent plate boundary (dashed green line in Figure 3G), synthetic pseudo-isochrons for each user-defined timestep (dashed black lines in Figure 3G), a current mid-ocean ridge (black line in Figure 3G), and curved but continuous transform fault/fracture zone tracks that result from Euler pole shifts (red lines in Figure 3G).

3.2 Additional Options

The mid-ocean ridge features developed by the code can be integrated as an evolving plate boundary in a plate tectonic model. To do so, these features can be combined with other features in GPlates, to manually create boundary topologies. There is also an option to let MORGen create plate boundary topologies. This option checks the plate boundary features per plate id for cross cutting and sorts the features in the right order to create a boundary topology. Boundary topologies may subsequently be used for further processing, such as input for the codes that compute paleo-age grids in self-closing plate polygons, i.e., gradually changing surface plates are defined from evolving intersecting plate boundaries (*Karlsen et al.*, 2020; *Merdith et al.*, 2019; *Seton et al.*, 2012; *Williams et al.*, 2021).

The MORGen algorithm can also create its own pseudo-isochrons at set time intervals based on the computed mid-ocean ridges. We thereby assume symmetric spreading, by means of half stage rotation. The algorithm can check pseudo-isochrons for subduction, formation of new plates and ridge jumps. This is done in three steps: (1) forward construction in time, starting from an approximate initial curvilinear ridge geometry; (2) assigning plate IDs to pseudo-isochrons at the reconstructed location (isochron features located in multiple plates are cut at this step); (3) check whether the plate ID of a pseudo-isochron has changed since the previous step. If the plate ID is unchanged, the feature continues its life as it is. If the plate ID has changed since the previous step there are two options (a) if the pseudo-isochron intersects a subduction zone feature, it is assumed to have subducted; (b) if it does not intersect a subduction zone, it is assumed to have changed to another plate, either by a ridge jump or by the break-up of an originally larger plate and the plate ID property is
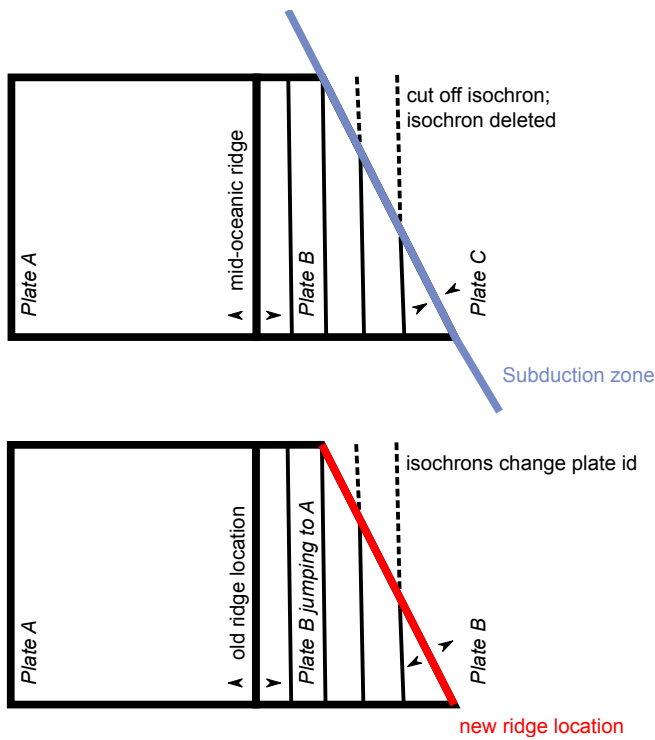
Figure 4 – Illustration of the procedure in which pseudo-isochrons generated by MORGen are clipped because they passed a subduction zone **(top)** or are reassigned a new plate ID because of a ridge jump **(bottom)**.

modified (Figure 4). If a too-small time step is chosen during an Euler pole shift and a pseudo-isochron is still located adjacent to a transform fault (instead of a within-plate fracture zone), rotation can then cause the pseudo-isochron to move over the transform fault and partially jump to the conjugate plate. In that case, the pseudo-isochron is deleted, and the age grid is computed from interpolation of remaining pseudo-isochrons.

Finally, the code can translate the pseudo-isochrons into age grids, and those into depth grids. The input parameters for the age grids are the coordinates and ages of points on the pseudo-isochrons. These are converted to a mean position on a grid and a mean value for age (with GMT blockmean). Subsequently empty blocks of the grid are filled with interpolated values (with GMT sphinterpolate). The age grid is converted to a bathymetry grid following Eq. 1 from (*Baatsen et al.*, 2016):

$$\begin{cases} Z_{a<90Ma} = 2620 + 330\sqrt{A} \\ Z_{A>90Ma} = 5750 \end{cases}, \qquad (1)$$

where Z is the basin depth in metres and A the ocean floor age in millions of years.

4 Proof of Concept

4.1 Simplified Input Model

Our algorithm aims to overcome the time-consuming procedures to create full plate models with mid-

ocean ridges that gradually adjust position during Euler pole shifts, but our approach obviously simplifies history. To illustrate the effects of this simplification, and explore potential pitfalls, we applied our code to predict an age grid for the South Atlantic and Southern Oceans, from which the age grid is well constrained by data. We use only the initial rift geometries and sets of Euler rotations constructed from marine magnetic anomalies. We drew the initial curves between Africa and South America using the fit of *Nürnberg and Müller* (1991) as referred to by *Torsvik et al.* (2009); also see *Owen-Smith et al.* (2019), for South America-Antarctica following the fit of *Müller et al.* (2019) and for Africa-Antarctica using the fit of *Müller et al.* (2019). We used the Euler poles describing the opening of the South Atlantic of *Müller et al.* (1999) and *Gaina et al.* (2013), and for Africa-Antarctica of *Royer and Chang* (1991); *Mueller and Jokat* (2019); *Cande et al.* (2010); *Bernard et al.* (2005). In the Weddell Sea, which opened due to South America-Antarctica spreading, only magnetic anomalies of the Antarctic plate remain (*Ghidella et al.*, 2002; *Mueller and Jokat*, 2019; *van de Lagemaat et al.*, 2021, and references therein). The South American conjugate set has been subducted at the South Sandwich subduction zone and its predecessors, since the Late Cretaceous (*van de Lagemaat et al.*, 2021, and references therein). Antarctica-South America motion in our model is inferred from the South America-Africa-Antarctica plate circuit.

South America-Africa motion is described using 17 Euler poles since approximately 140 Ma. In the same period Antarctica-Africa motion is described with 32 Euler poles, signalling a total of 47 Euler pole shifts. The 'traditional' approach thus required redrawing the ridge-transform system 47 times and defining self-closing plate boundaries after each shift. Below we assess when and where our simplified approach mispredicts the documented ages and geometries of the South Atlantic and Southern Ocean sea floor.

4.2 Test Against Real World Data: Proof of Concept

The MORGen algorithm created synthetic pseudo-isochrons for the test area (Figure 5). Curvilinear rifts serve as input features for the simplified model (Figure 5A), with some simplified plate boundary features to geometrically close the plate boundaries. Figure 5B shows all the created pseudo-isochrons and the plate boundary topologies as created by the algorithm. This does not take into account subduction, ridge jumps, or the creation of new plates through break up. Figure 5C shows the pseudo-isochrons after the check for change of plate id. Of interest is here that the pseudo-isochrons not inside a closed plate boundary have been removed, as would subducted pseudo-isochrons; the ridge jump in the southern part of the South Atlantic that transfers the 'Malvinas Plate' from South America to Africa is shown correctly, and pseudo-isochrons created as part of the South American plate have been transferred to the
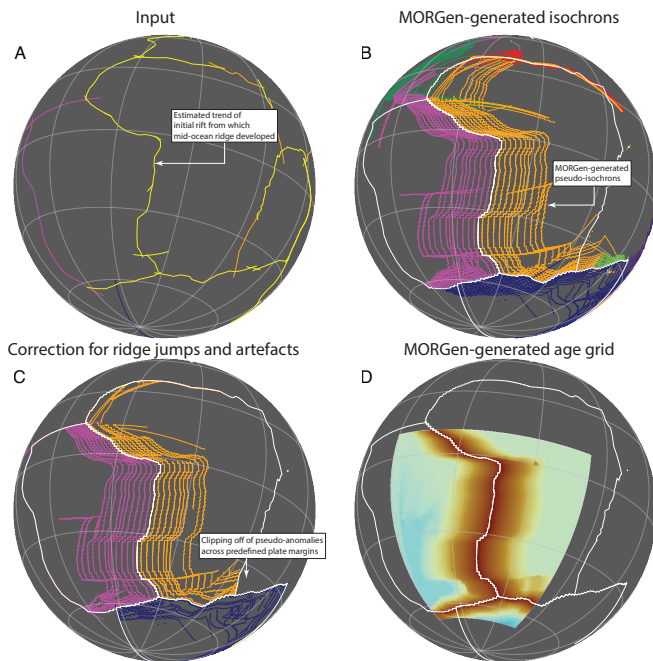
Figure 5 – **A)** input features, mid-ocean ridges in yellow; other features coloured with plate id (relevant plates: South America is magenta, Africa is orange, Antarctica is blue; features required to create full plate boundaries also produce pseudo-isochrons in other colours which are not relevant for the southern ocean). **B)** synthetic pseudo-isochrons and plate boundary topologies created by the algorithm; **C)** synthetic pseudo-isochrons after check for change of plate id (subduction, ridge jump or creation of new plate); **D)** age grid calculated from synthetic pseudo-isochrons.

African plate by a ridge jump (we note that detailed study has shown that this transfer likely involved a protracted period of time (*Marks and Stock*, 2001), and the discrete ridge jump is a simplification). In Figure 5C (parts of) pseudo-isochrons have disappeared due to cutting the mid-ocean ridge shortly after their creation. Figure 5D shows an age grid calculated from the pseudo-isochrons.

Zooming in, the pseudo-isochrons show smooth transitions in orientation at Euler pole shifts (Figure 6), with adjustments in spreading centre orientation and transform fault orientation and segment spacing. A visual comparison between the synthetic pseudo-isochrons from our model with observed fracture zones (*Seton et al.*, 2012) shows a good fit in key areas (Figure 6). The fracture zones line up with the transform segments of the synthetic pseudo-isochrons in most places. Obviously, these fracture zones have been used as input to determine the Euler poles that we used to compute the pseudo-fracture zones and pseudo-isochrons, but the good fit shows that our model reproduces the input data well. Minor mismatches may have an underlying geological reason, reflecting small-scale relative motions between the conjugate sea floor of the Weddell Sea and the South American plate that was recently inferred by *van de Lagemaat et al.* (2021).

A visual comparison (Figure 7) between age grids computed with our model and detailed age grids based on marine magnetic anomaly reconstructions from *Seton et al.* (2020) shows that our prediction yields similar results, as illustrated in Figure 7C. Also, the ridge jump in the southeastern Atlantic Ocean, which around 65 Ma merged the 'Malvinas Plate' that was originally part of the South American plate with Africa, is reconstructed. Please note that the Scotia Sea (bottom left area) was not included in our reconstruction model. The MORGen-generated prediction shows less prominent fracture zones than the *Seton et al.* (2020) grid, which has the natural, higher variation, more clearly showing the approximately 500 km scale sections with transforms. The smoothing in our model is further caused by the interpolation which is done on a grid without consideration of fracture zones. For better results, the mid-ocean ridges features generated by MORGen could be used as input for algorithms that are better at creating age grids, such as *Karlsen et al.* (2020); *Merdith et al.* (2019); *Seton et al.* (2012); *Williams et al.* (2021).

4.3   Example Applications

We illustrate the MORGen algorithm by generating two ridges in (re)constructions of ocean basins. The first example portrays the complex ocean basins that formed in Triassic to early Cretaceous time in the Mediterranean region as reconstructed by *van Hinsbergen et al.* (2020) (Figure 8). Almost all these ocean basins have since subducted and are reconstructed based on relics exposed in Mediterranean orogens, and kinematic restoration of the exposed fold-thrust belts in context of the Eurasia-North America-Africa plate circuit. The reconstruction infers that during the Triassic a series of ocean basins formed within the north Gondwana margin and after a series of ridge jumps, a larger 'Neotethyan' ocean basin opened. The reconstruction, moreover, contains several Euler pole shifts. Each ridge jump and Euler pole shift would normally require redrawing of the ridge. Figure 8 illustrates the pseudo-isochrons constructed using the MORGen algorithm for this reconstruction, which followed from the constructed initial rifts. Finally, we illustrate the tool with a recent construction of an ocean in a future supercontinent (Figure 9). This construction is based on a future continental drift model of Davies et al. (2018), to which plate boundaries and orogenic constructions were added by *van Hinsbergen and Schouten* (2021). In this scenario, the East African Rift develops into a mid-ocean ridge, creating the African Ocean and is associated with one Euler pole shift (Figure 9). These examples illustrate the straightforward application of the MORGen algorithm, which makes for user-friendly, easily updatable pseudo-isochron and age grid (re)constructions.

5   Conclusions

In this paper, we present the Mid-Ocean Ridge Generator (MORGen) algorithm to automate the laborious, manual procedure of creating mid-ocean ridge features, spreading centre and transform fault seg-
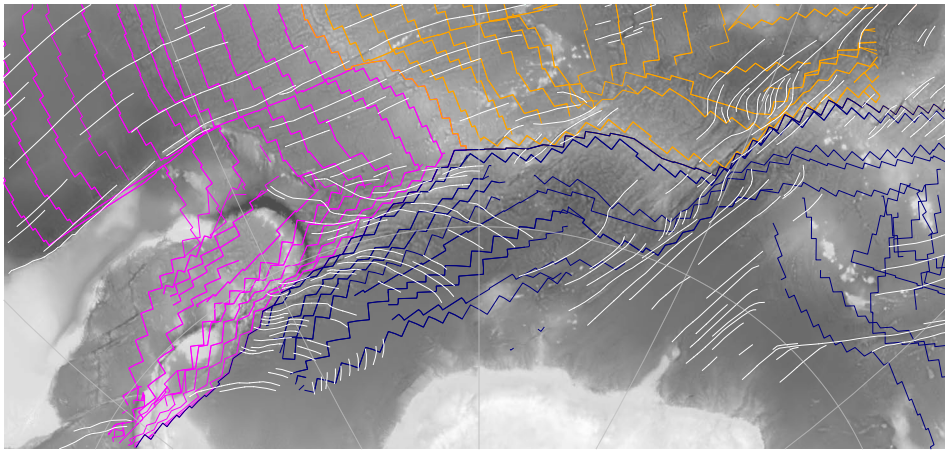
Figure 6 – Bathymetry (from ETOPO) in grey scale as background; fracture zones from *Seton et al.* (2020) in white and synthetic pseudo-isochrons from our model coloured per plate id (blue: Antarctica, orange: Africa, pink: South America).
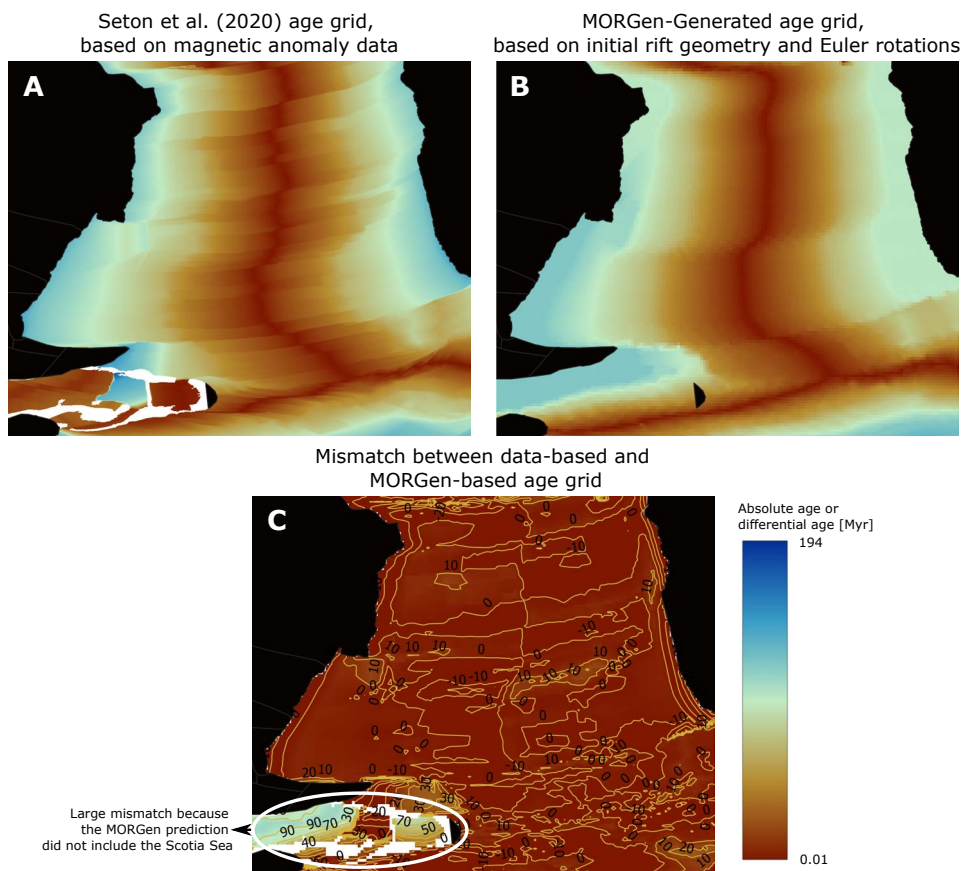

Figure 7 – Present day age grids in the South Atlantic and Southern Oceans. **A)** 2020.1.GeeK2007 (*Seton et al.*, 2020); **B)** our model; **C)** differential ages between the two. Note that our model did not include a Scotia Sea reconstruction. The large age differences computed there are the difference between the predicted age of the now-subducted lithosphere present in our model, and the present-day lithosphere in the Scotia Sea present in the *Seton et al.* (2020) model.

ment in full-plate reconstructions for modelled ocean basins from which no lithosphere is present in the modern oceans. The algorithm uses curved line features representing approximate initial rift geometries as input and develops these into typical stepped ridge-transform geometries with a user-defined, but default ~70 km spacing between transforms. Upon Euler pole shifts, the initial ridge geometries are maintained – as demonstrated in nature on the modern ocean floor – and transform and spreading centre orientation and spacing are adjusted according to

the new Euler pole. The MORGen algorithm allows for straightforward reconstruction of mid-ocean ridges in full-plate models, and paleo-age grids computed from those. We show that our synthetic construction of the South Atlantic ocean floor from a single, simple initial rift geometry provides a smoothed, but otherwise accurate reproduction of the geophysically constrained modern ocean floor.
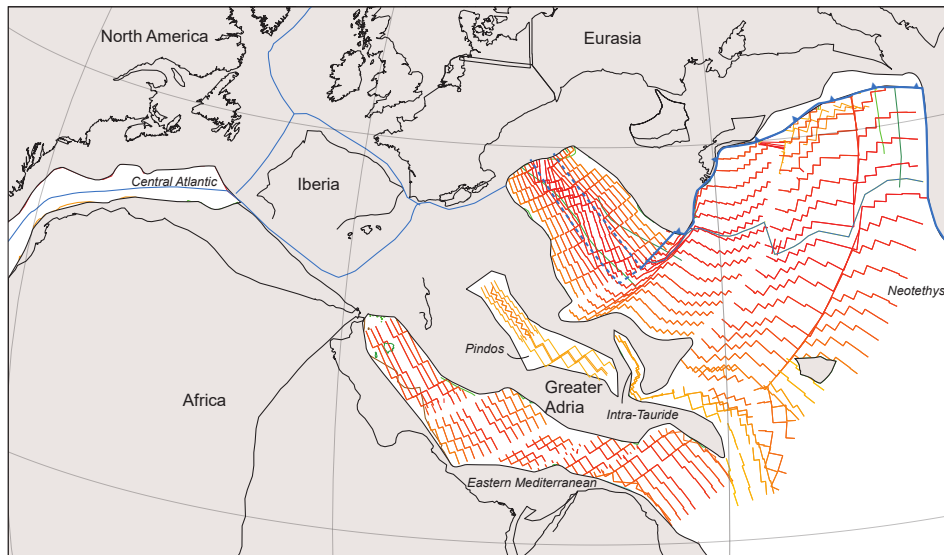
Figure 8 – Pseudo-Isochrons computed for the Mediterranean region for a time slice at 170 Ma, using the MORGen code, and Euler poles predicted for the opening of these basins derived from *van Hinsbergen et al.* (2020). Pseudo-isochrons created at 5 Myr intervals, coloured from orange (oldest) to red (youngest). Plate boundaries coloured blue, active mid ocean ridges coloured green.
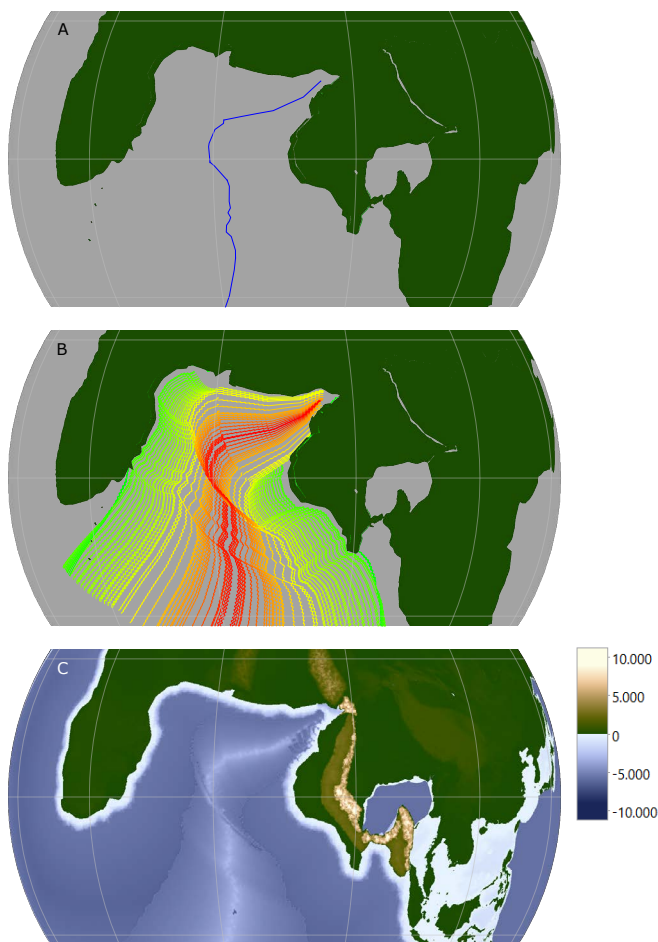

Figure 9 – Model for future prediction at 200 Ma into the future (*van Hinsbergen and Schouten*, 2021). **A)** input with mid-ocean ridge in blue, continents in green; **B)** synthetic pseudo-isochrons at 5 Myr intervals created with the model, coloured by age from green (oldest) to red (youngest); **C)** digital elevation model based on the pseudo-isochrons.

Acknowledgements

Author contributions

Thomas J. M. van der Linden: conceptualisation, software, visualisation, writing.
Douwe J. J. van Hinsbergen: conceptualisation, visualisation, writing.

Data and software availability

The code used in this work is called MORGen (Mid-Ocean Ridge Generator). It was developed by Thomas J.M. van der Linden (e-mail: thomas@lingeo.eu) and first time made available in 2021. The code requires Python 3.7, including standard libraries, GMT version 6, and the Python libraries: pyGPlates revision 28 and NumPy. Source code is available for downlowd from https://bitbucket.org/thovdl/-morgen/. Data used in this work can be downloaded from https://bitbucket.org/thovdl/morgen/src/main/data/raw/plateReconstructions/.

Competing interests

The authors declare no competing interests.

Peer review

This publication was peer-reviewed by John Cannon, Lucia Perez-Diaz, and an anonymous reviewer. The full peer-review report can be found here: https://tektonika.online/index.php/home/article/view/14/24

Copyright notice

References

Atwater, T., and K. C. Macdonald (1977), Are spreading centers perpendicular to their transform faults?, *Nature*, *270*(5639), 715–719, doi: 10.1038/270715a0.

Baatsen, M., D. J. J. van Hinsbergen, A. S. Von Der Heydt, H. A. Dijkstra, A. Sluijs, H. A. Abels, and P. K. Bijl (2016), Reconstructing geographical boundary conditions for palaeoclimate modelling during the Cenozoic, *Climate of the Past*, *12*(8), 1635–1644, doi: 10.5194/cp-12-1635-2016.

Bernard, A., M. Munschy, Y. Rotstein, and D. Sauter (2005), Refined spreading history at the Southwest Indian Ridge for the last 96 Ma, with the aid of satellite gravity data, *Geophysical Journal International*, *162*(3), 765–778, doi: 10.1111/j.1365-246X.2005.02672.x.

Bird, P. (2003), An updated digital model of plate boundaries, *Geochemistry, Geophysics, Geosystems*, *4*(3), doi: 10.1029/2001GC000252.

Boschman, L. M., and D. J. J. van Hinsbergen (2016), On the enigmatic birth of the Pacific Plate within the Panthalassa Ocean, *Science Advances*, *2*(7), doi: 10.1126/sciadv.1600022.

Bosworth, W. (1985), Geometry of propagating continental rifts, *Nature*, *316*(6029), 625–627, doi: 10.1038/316625a0.

Boyden, J. A., R. D. Müller, M. Gurnis, T. H. Torsvik, J. A. Clark, M. Turner, H. Ivey-Law, R. J. Watson, and J. S. Cannon (2011), Next-generation plate-tectonic reconstructions using GPlates, in *Geoinformatics*, edited by G. R. Keller and C. Baru, pp. 95–114, Cambridge University Press, Cambridge, doi: 10.1017/cbo9780511976308.008.

Cande, S. C., P. Patriat, and J. Dyment (2010), Motion between the Indian, Antarctic and African plates in the early Cenozoic, *Geophysical Journal International*, *183*(1), 127–149, doi: 10.1111/j.1365-246X.2010.04737.x.

Cox, A., and R. B. Hart (1986), *Plate Tectonics : How It Works*, Wiley-Blackwell.

Domeier, M. (2016), A plate tectonic scenario for the Iapetus and Rheic oceans, *Gondwana Research*, *36*, 275–295, doi: 10.1016/j.gr.2015.08.003.

Domeier, M. (2018), Early Paleozoic tectonics of Asia: Towards a full-plate model, *Geoscience Frontiers*, *9*(3), 789–862, doi: 10.1016/j.gsf.2017.11.012.

Domeier, M., and T. H. Torsvik (2014), Plate tectonics in the late Paleozoic, *Geoscience Frontiers*, *5*(3), 303–350, doi: 10.1016/j.gsf.2014.01.002.

Domeier, M., and T. H. Torsvik (2019), Full-plate modelling in pre-Jurassic time, *Geological magazine*, *156*(2), 261–280, doi: 10.1017/S0016756817001005.

Gaina, C., T. H. Torsvik, D. J. J. van Hinsbergen, S. Medvedev, S. C. Werner, and C. Labails (2013), The African Plate: A history of oceanic crust accretion and subduction since the Jurassic, *Tectonophysics*, *604*, 4–25, doi: 10.1016/j.tecto.2013.05.037.

Gerya, T. (2010), Dynamical instability produces transform faults at mid-ocean ridges, *Science*, *329*(5995), 1047–1050, doi: 10.1126/science.1191349.

Ghidella, M. E., G. Yáñez, and J. L. LaBrecque (2002), Revised tectonic implications for the magnetic anomalies of the western Weddell Sea, *Tectonophysics*, *347*(1-3), 65–86, doi: 10.1016/S0040-1951(01)00238-4.

Guan, Q., T. Zhang, B. Taylor, J. Gao, and J. Li (2021), Ridge jump reorientation of the South China Sea revealed by high-resolution magnetic data, *Terra Nova*, *33*(5), 475–482, doi: 10.1111/ter.12532.

Gurnis, M., T. Yang, J. Cannon, M. Turner, S. Williams, N. Flament, and R. D. Müller (2018), Global tectonic reconstructions with continuously deforming and evolving rigid plates, *Computers and Geosciences*, *116*, 32–41, doi: 10.1016/j.cageo.2018.04.007.

Karlsen, K. S., M. Domeier, C. Gaina, and C. P. Conrad (2020), A tracer-based algorithm for automatic generation of seafloor age grids from plate tectonic reconstructions, *Computers and Geosciences*, *140*, 1–20, doi: 10.1016/j.cageo.2020.104508.

Labrecque, J. L., and D. E. Hayes (1979), Seafloor spreading history of the Agulhas Basin, *Earth and planetary science letters*, *45*(2), 411–428, doi: 10.1016/0012-821X(79)90140-7.

Luhr, J. F., S. A. Nelson, J. F. Allan, and I. S. E. Carmichael (1985), Active rifting in southwestern Mexico: Manifestations of an incipient eastward spreading-ridge jump, *Geology*, *13*(1), 54, doi: 10.1130/0091-7613(1985)13<54:ARISMM>2.0.CO;2.

Marks, K. M., and J. M. Stock (2001), Evolution of the Malvinas Plate South of Africa, *Marine Geophysical Researches*, *22*(4), 289–302, doi: 10.1023/A:1014638325616.

Matthews, K. J., K. T. Maloney, S. Zahirovic, S. E. Williams, M. Seton, and R. D. Müller (2016), Global plate boundary evolution and kinematics since the late Paleozoic, *Global and planetary change*, *146*, 226–250, doi: 10.1016/j.gloplacha.2016.10.002.

McKenzie, D. P., and R. L. Parker (1967), The North Pacific: an Example of Tectonics on a Sphere, *Nature*, *216*(5122), 1276–1280, doi: 10.1038/2161276a0.

Menard, H. W., and T. Atwater (1968), Changes in direction of sea floor spreading, *Nature*, *219*(5153), 463–467, doi: 10.1038/219463a0.

Merdith, A. S., A. S. Collins, S. E. Williams, S. Pisarevsky, J. D. Foden, D. B. Archibald, M. L. Blades, B. L. Alessio, S. Armistead, D. Plavsa, C. Clark, and R. D. Müller (2017), A full-plate global reconstruction of the Neoproterozoic, *Gondwana Research*, *50*, 84–134, doi: 10.1016/j.gr.2017.04.001.

Merdith, A. S., S. E. Atkins, and M. G. Tetley (2019), Tectonic Controls on Carbon and Serpentinite Storage in Subducted Upper Oceanic Lithosphere for the Past 320 Ma, *Frontiers of Earth Science in China*, *7*, doi: 10.3389/feart.2019.00332.

Merdith, A. S., S. E. Williams, A. S. Collins, M. G. Tetley, J. A. Mulder, M. L. Blades, A. Young, S. E. Armistead, J. Cannon, S. Zahirovic, and R. D. Müller (2021), Extending full-plate tectonic models into deep time: Linking the Neoproterozoic and the Phanerozoic, *Earth-Science Reviews*, *214*, 103,477, doi: 10.1016/j.earscirev.2020.103477.

Morgan, W. J. (1991), Rises, Trenches, Great Faults and Crustal Blocks, *Tectonophysics*, *187*(1-3), 6–22, doi: 10.1016/0040-1951(91)90408-K.

Mueller, C. O., and W. Jokat (2019), The initial Gondwana break-up: A synthesis based on new potential field data of the Africa-Antarctica Corridor, *Tectonophysics*, *750*, 301–328, doi: 10.1016/j.tecto.2018.11.008.

Müller, R. D., J.-Y. Royer, S. C. Cande, W. R. Roest, and S. Maschenkov (1999), Chapter 2 New constraints on the late cretaceous/tertiary plate tectonic evolution of the caribbean, in *Sedimentary Basins of the World*, vol. 4, edited by P. Mann, pp. 33–59, Elsevier, doi: 10.1016/S1874-5997(99)80036-7.

Müller, R. D., M. Seton, S. Zahirovic, S. E. Williams, K. J. Matthews, N. M. Wright, G. E. Shephard, K. T. Maloney, N. Barnett-Moore, M. Hosseinpour, D. J. Bower, and J. Cannon (2016), Ocean Basin Evolution and Global-Scale Plate Reorganization Events Since Pangea Breakup, *Annual review of earth and planetary sciences*, *44*(1), 107–138, doi: 10.1146/annurev-earth-060115-012211.

Müller, R. D., J. Cannon, X. Qin, R. J. Watson, M. Gurnis, S. Williams, T. Pfaffelmoser, M. Seton, S. H. J. Russell, and S. Zahirovic (2018), GPlates: Building a Virtual Earth Through Deep Time, *Geochemistry, Geophysics, Geosystems*, *19*(7), 2243–2261, doi: 10.1029/2018GC007584.

Müller, R. D., S. Zahirovic, S. E. Williams, J. Cannon, M. Seton, D. J. Bower, M. G. Tetley, C. Heine, E. Le Breton, S. Liu, S. H. J. Russell, T. Yang, J. Leonard, and M. Gurnis (2019), A Global Plate Model Including Lithospheric Deformation Along Major Rifts and Orogens Since the Triassic, *Tectonics*, *38*(6), 1884–1907, doi: 10.1029/2018TC005462.

Nürnberg, D., and R. D. Müller (1991), The tectonic evolution of the South Atlantic from Late Jurassic to present, *Tectonophysics*, *191*(1-2), 27–53, doi: 10.1016/0040-1951(91)90231-G.

Owen-Smith, T. M., M. Ganerød, D. J. J. van Hinsbergen, C. Gaina, L. D. Ashwal, and T. H. Torsvik (2019), Testing Early Cretaceous Africa–South America fits with new palaeomagnetic data from the Etendeka Magmatic Province (Namibia), *Tectonophysics*, *760*, 23–35, doi: 10.1016/j.tecto.2017.11.010.

Royer, J.-Y., and T. Chang (1991), Evidence for Relative Motions Between the Indian and Australian Plates During the Last 20 m.y. From Plate Tectonic Reconstructions' Implications for the Deformation of the Indo-Australian Plate, *Journal of geophysical research*, *96*(B7), 11,779–11,802.

Seton, M., R. D. Müller, S. Zahirovic, C. Gaina, T. Torsvik, G. Shephard, A. Talsma, M. Gurnis, M. Turner, S. Maus, and M. Chandler (2012), Global continental and ocean basin reconstructions since 200Ma, *Earth-Science Reviews*, *113*(3-4), 212–270, doi: 10.1016/j.earscirev.2012.03.002.

Seton, M., R. D. Müller, S. Zahirovic, S. Williams, N. M. Wright, J. Cannon, J. M. Whittaker, K. J. Matthews, and R. McGirr (2020), A Global Data Set of Present-Day Oceanic Crustal Age and Seafloor Spreading Parameters, *Geochemistry, Geophysics, Geosystems*, *21*(10), doi: 10.1029/2020GC009214.

Torsvik, T. H., and L. R. M. Cocks (2016), *Earth History and Palaeogeography*, 1–332 pp., Cambridge University Press, doi: 10.1017/9781316225523.

Torsvik, T. H., S. Rousse, C. Labails, and M. A. Smethurst (2009), A new scheme for the opening of the South Atlantic Ocean and the dissection of an Aptian salt basin, *Geophysical Journal International*, *177*(3), 1315–1333, doi: 10.1111/j.1365-246X.2009.04137.x.

Unidata (2021), Network Common Data Form (netCDF), doi: 10.5065/D6H70CW6.

van de Lagemaat, S. H. A., M. L. A. Swart, B. Vaes, M. E. Kosters, L. M. Boschman, A. Burton-Johnson, P. K. Bijl, W. Spakman, and D. J. J. van Hinsbergen (2021), Subduction initiation in the Scotia Sea region and opening of the Drake Passage: When and why?, *Earth-Science Reviews*, *215*, 103,551, doi: 10.1016/j.earscirev.2021.103551.

van Hinsbergen, D. J. J., and T. L. A. Schouten (2021), Deciphering paleogeography from orogenic architecture: Constructing orogens in a future supercontinent as thought experiment, *American journal of science*, *321*(6), 955–1031, doi: 10.2475/06.2021.09.

van Hinsbergen, D. J. J., T. H. Torsvik, S. M. Schmid, L. C. Maţenco, M. Maffione, R. L. M. Vissers, D. Gürer, and W. Spakman (2020), Orogenic architecture of the Mediterranean region and kinematic reconstruction of its tectonic evolution since the Triassic, *Gondwana Research*, *81*, 79–229, doi: 10.1016/j.gr.2019.07.009.

Van Rossum, G., and F. L. Drake (2011), *The python language reference manual*, Network Theory Ltd.

Wessel, P., W. H. F. Smith, R. Scharroo, J. Luis, and F. Wobbe (2013), Generic Mapping Tools: Improved Version Released, *Eos, Transactions, American Geophysical Union*, *94*(45), 409–410, doi: 10.1002/2013EO450001.

Williams, S., N. M. Wright, J. Cannon, N. Flament, and R. D. Müller (2021), Reconstructing seafloor age distributions in lost ocean basins, *Geoscience Frontiers*, *12*(2), 769–780, doi: 10.1016/j.gsf.2020.06.004.

Wilson, J. T. (1965), A new class of faults and their bearing on continental drift, *Nature*, *207*(4995), 343–347, doi: 10.1038/207343a0.

Young, A., N. Flament, K. Maloney, S. Williams, K. Matthews, S. Zahirovic, and R. D. Müller (2018), Global kinematics of tectonic plates and subduction zones since the late Paleozoic Era, *Geoscience Frontiers*, *10*(3), 989–1013, doi: 10.1016/j.gsf.2018.05.011.